Methods 168 (2019) 40–50

Contents lists available at ScienceDirect

Methods

journal homepage: www.elsevier.com/locate/ymeth

Fluorescent probes with high pKa values based on traditional, near-infrared rhodamine, and hemicyanine fluorophores for sensitive detection of lysosomal pH variations

Wafa Mazi, Rashmi Adhikari, Yibin Zhang, Shuai Xia, Mingxi Fang, Rudy L. Luck, Momoko Tajiri, Ashutosh Tiwari, Marina Tanasova, Haiying Liu

Department of Chemistry, Michigan Technological University, Houghton, MI 49931, United States

ARTICLE INFO

Keywords:
Fluorescent probes
Near-infrared fluorescence
Rhodamine dyes
Lysosomal pH
Fluorescence imaging

ABSTRACT

Sterically hindered fluorescent probes (**A**-**C**) have been developed by introducing 2-aminophenylboronic acid pinacol ester to a traditional, **A**, a near-infrared rhodamine dye, **B**, and a near-infrared hemicyanine dye, **C**, forming closed spirolactam ring structures. Probe **A** was non-fluorescent under basic pH conditions whereas probes **B** and **C** were moderately fluorescent with fluorescence quantum yields of 9% and 5% in pH 7.4 PBS buffer containing 1% ethanol, respectively. With all probes increasing acidity leads to significant increases in fluorescence at 580 nm, 644 and 744 nm for probes **A**, **B** and **C** with fluorescence quantum yields of 26%, 21% and 10% in pH 4.5 PBS buffer containing 1% ethanol, respectively. Probes **A**, **B** and **C** were calculated to have pK_a values of 5.81, 5.45 and 6.97. The difference in fluorescence under basic conditions is ascribed to easier opening of the closed spirolactam ring configurations due to significant steric hindrance between the 2-aminophenylboronic acid pinacol ester residue and an adjacent H atom in the xanthene derivative moiety in probe **B** or **C**. The probes show fast, reversible, selective and sensitive fluorescence responses to pH changes, and are capable of sensing lysosomal pH variations in living cells.

1. Introduction

Various cellular processes including cell proliferation, cell growth, apoptosis, signal transduction, and cellular metabolism are very dependent on intracellular pH levels [1-8]. Any pH variance from normal levels are often associated with cellular dysfunctions and serious diseases such as cancer and Alzheimer's [1,3,6,9,10]. The pH values inside cancer cells are different from those in normal cells [11]. For example, the extracellular pH (pH_{ex}) of tumor tissues is often acidic and at pH values between 6.2 and 6.9. Lysosomes function to break down biological molecules under acidic pH values from 4.0 to 6.0 [12,13]. Abnormal lysosomal pH can lead to lysosomal storage disorders. Therefore, accurate determinations of intracellular pH values are important in order to understanding various physical, biological and pathological progressions. Many fluorescent probes have been developed for detection of intracellular pH and they normally demonstrate high sensitivity, selectivity, real-time spatial imaging, minimal damaging effects, and simplicity of operation [12–18]. Traditional rhodamine dyes and their near-infrared derivatives have been used to develop fluorescent probes based on spirolactam molecular switches for pH detection in living cells because of their outstanding photophysical properties including high molar extinction coefficients, high fluorescence quantum yield, excellent photostability, and a large signal-to-background ratio [7,14-17,19–25]. Different amine-functionalized alkane bearing different functional groups and oligo(ethylene glycol) derivatives have been introduced to rhodamine and its derivatives to form closed spirolactam ring structures.[8,14,15,17,26,27] However, these fluorescent probes are highly fluorescent under acidic conditions and are non-fluorescent under neutral and basic pH conditions. Introducing steric hindrance by attaching bulky residues such as amine-functionalized adamantly molecules and different aniline derivatives such as o-phenylenediamine, 2,6-dichloroamiline, 2,6-diethoxyaniline, 2-propylamine and 2,6-dipropylaniline to traditional rhodamine and derivatives to facilitate acid-activated opening of the closed spirolactam rings at higher pKa values has been studied.[23,25,28,29] However, most fluorescent probes with closed spirolactam molecular switches are still non-fluorescent under basic pH conditions [7,21–26]. Therefore, it is important to overcome the non-fluorescent limitation of these fluorescent probes with closed spirolactam switches under basic pH conditions in order to take advantage of the outstanding photophysical properties of

E-mail addresses: rluck@mtu.edu (R.L. Luck), mtajiri@mtu.edu (M. Tajiri), tiwari@mtu.edu (A. Tiwari), mtanasov@mtu.edu (M. Tanasova), hyliu@mtu.edu (H. Liu).

https://doi.org/10.1016/j.ymeth.2019.07.012
Received 29 March 2019; Received in revised form 11 July 2019; Accepted 12 July 2019
Available online 22 July 2019

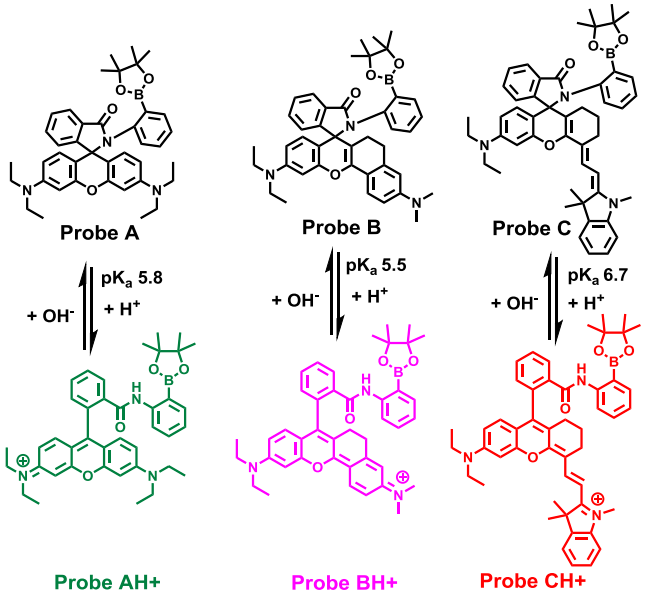

Scheme 1. Chemical structures of fluorescent probes in responses to pH changes.

rhodamine and its derivatives.

In this article, we detail the design and syntheses of three fluorescent probes (**A–C**), Scheme 1, bearing closed spirolactam ring configurations with high pK$_a$ values for lysosomal pH detection in living cells by introducing a significantly sterically bulky 2-aminophenylboronic acid pinacol ester to traditional rhodamine B and its near-infrared derivative, and near-infrared hemicyanine dyes, respectively, in order to improve the spectroscopic properties of the dyes. We chose 2-aminophenylboronic acid pinacol ester instead of its derivatives such as 3-aminophenylboronic acid pinacol ester and 4-aminophenylboronic acid pinacol ester to significantly enhance steric hindrance between the closed spirolactam ring and xanthene cores to considerably increase pK$_a$ values related to opening of the spirolactam ring structures. Probes **B** and **C** based on near-infrared rhodamine and hemicyanine dyes, with pKa values of 5.45 and 6.97, display significant fluorescence peaks at 644 nm and 744 nm under basic pH level of 8.8, respectively. The higher pKa value in probe C compared to that for probe **B** may be due to increased steric hindrance as noted above. Probe **A** similar to fluorescent probes based on traditional rhodamine dyes is non-fluorescent with a pKa value of 5.81 under basic pH conditions. Probes **B** and **C** display activated fluorescent responses to both acidic and basic intracellular pH ranges and are capable of monitoring acidic pH variations in lysosomes.

2. Experimental section

2.1. Materials

Unless specifically indicated, all reagents and solvents were obtained from commercial suppliers and used without further purification.

2.1.1. Synthesis of fluorescent probe *A*

Rhodamine B (0.498 g, 1.04 mmol) was dissolved in 10 mL of dry dichloromethane, Bop reagent (0.707 g, 1.6 mmol) and 0.5 mL of trimethylamine were added to the solution. After the reaction was stirred for 30 min, 2-aminophenylboronic acid pinacol ester (0.300 g,

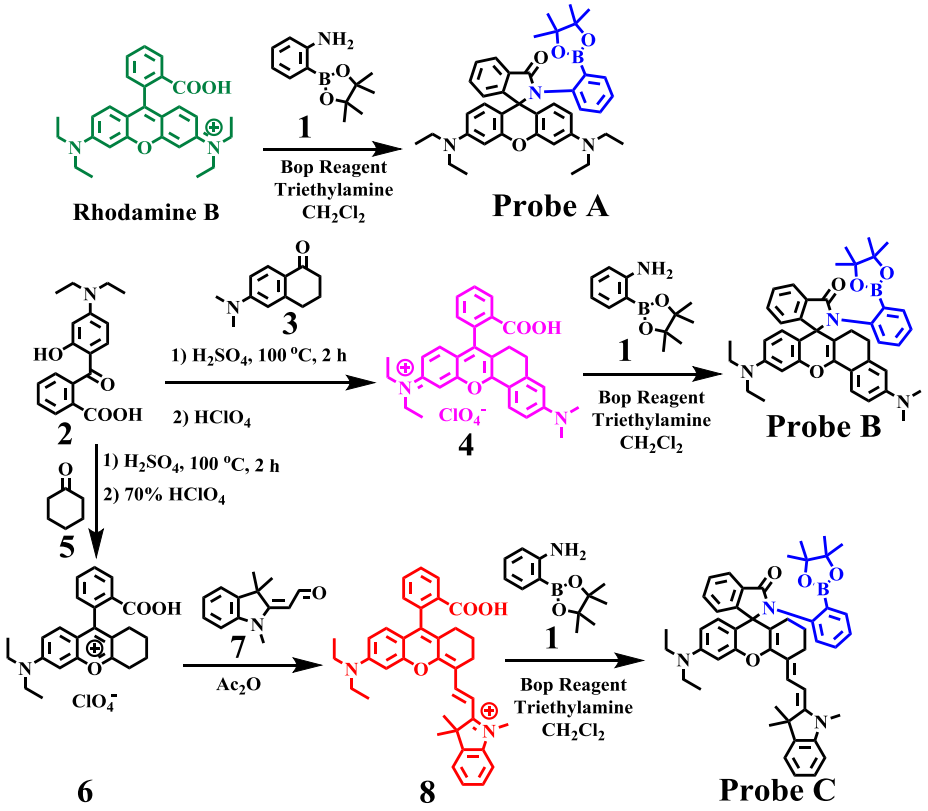

Scheme 2. Synthetic approach to prepare fluorescent probes **A**, **B**, **and C**.

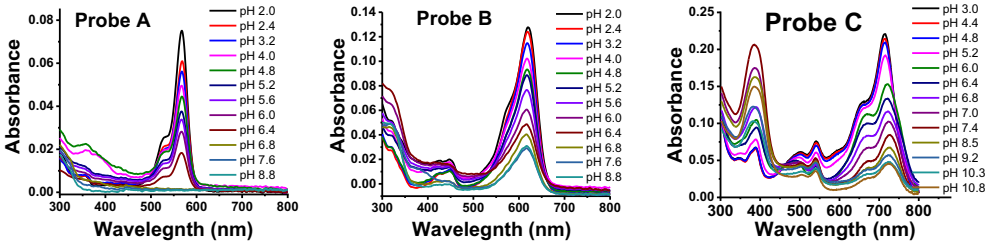

Fig. 1. Absorption spectra of 5 μM probes **A**, **B**, and **C** and their respective protonated versions in different pH buffers containing 1% ethanol. Citrate-phosphate buffers were used for pH values from 2.0 to 7.0 while phosphate buffers were employed for pH values from 7.0 to 10.8.

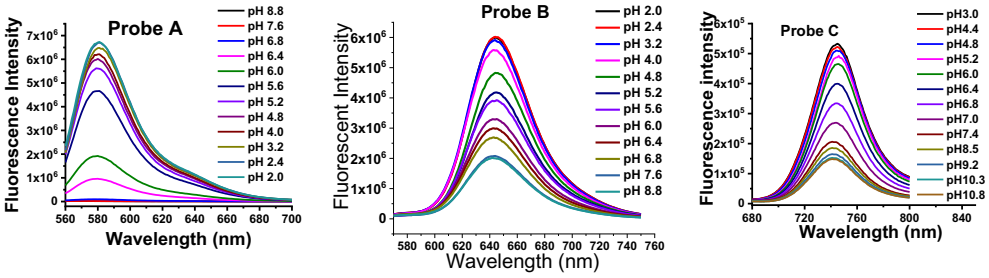

Fig. 2. Fluorescence spectra of 5 μM probes **A**, **B**, and **C** in different pH buffers containing 1% ethanol after excitation at 530 nm, 560 nm, and 660 nm, respectively. Citrate-phosphate buffers were used for pH values from 2.0 to 7.0 while phosphate buffers were employed for pH values from 7.0 to 10.8.

1.36 mmol) was added to the reaction mixture, the reaction mixture was stirred overnight at room temperature under a nitrogen atmosphere. The solvent was removed from the reaction mixture and the crude product purified by column chromatography using a four solvent system hexane/methylene chloride/ethyl acetate/MeOH 5/3/1/0.18 resulting in the product as a light pink solid with 58% yield.

^{1}HNMR (400 MHz, $CDCl_3$) δ: 7.99 (1H, d, J = 6.88), 7.71 (1H, dd, J = 5.92), 7.50 (3H, m), 7.09 (2H, m), 6.92 (1H, m), 6.59 (1H, d, J = 8.2), 6.57 (1H, d, J = 8.88), 6.42 (2H, d, J = 2.44), 6.14 (2H, dd, J = 2.52), 3.31 (8H, q, J = 7.08, 7.17), 1.44 (12H , s), 1.15 (13H, m); ^{13}C NMR (75 MHz, $CDCl_3$) δ: 167.54, 154.89, 152.15, 149.12, 131.57, 128.39, 127.98, 127.57, 126.71, 125.85, 123.59, 123.35, 116.58, 108.22, 104.42, 98.05, 80.96, 69.89, 44.46, 29.88, 26.44, 25.11, 12.78.

2.1.2. Synthesis of fluorescent probe *B*

Near-infrared rhodamine dye (**4**) was prepared by the condensation of 6-(dimethylamino)-3,4-dihydronaphthalen-1(2H)-one (**3**) with 2-(4-(diethylamino)-2-hydroxybenzoyl)benzoic acid in sulfuric acid at high temperature according to the literature [30]. Near-infrared rhodamine dye (**4**) (100.0 mg, 0.21 mmol) was then dissolved in 5 mL of dry dichloromethane, trimethylamine 0.5 mL and Bop (140 mg, 0.32 mmol) added and the mixture stirred for 15 min. 2-Aminophenylboronic acid pinacol ester (95.0 mg, 0.21 mmol) was dissolved in 2 mL of dichloromethane and added to the reaction mixture and stirred at room temperature overnight under N_2. The solvent was removed and crude was washed with water, extracted with dichloromathane and dried over anhydrous sodium sulfate. The solvent was evaporated and the crude product was purified by column chromatography with dichloromethane/methanol (v/v) 50:1 and then (v/v) 20:1 producing the product as a blue solid in 20% yield.

^{1}HNMR (400 MHz, Acetonitrile-d_3) δ: 10.20 (1H, s), 8.21 (1H, d, J = 8.4), 8.15 (1H, m), 8.07 (1H, m), 7.79 (2H, m), 7.72 (1H, m), 7.60 (1H, m), 7.53 (1H, m), 7.33 (1H, m), 7.05 (1H, m), 6.86 (1H, d, J = 2.48), 6.80 (2H, m), 6.47 (1H, d, J = 2.48), 3.54 (4H, q, J = 7.24 and 7.24), 3.16 (4H, s), 2.87 (6H, s,s), 2.64 (4H, q, J = 9.12 and 8.88), 1.40 (12H, d, J = 2.92), 1.27 (6H, m); ^{13}CNMR (75 MHz, Acetonitrile-d_3) δ: 164.51, 164.27, 158.99, 156.83, 155.42, 153.49, 145.52, 144.27, 136.57, 135.37, 134.03, 133.03, 132.18, 131.27, 129.97, 129.84, 129.34, 127.04, 126.42, 123.78, 120.97, 119.33, 115.20, 114.88, 112.28, 110.75, 107.88, 96.43, 85.01, 45.79, 40.66, 37.80, 37.76, 37.12, 31.23, 30.00, 28.06,25.33, 25.29, 24.39, 12.80.

2.1.3. Synthesis of fluorescent probe *C*

Near-infrared hemicyanine dye (**8**) were prepared by the condensation of Fisher aldehyde (**7**) with 9-(2-carboxyphenyl)-6-(diethylamino)-1,2,3,4-tetrahydroxanthylium percloride (**6**) [31–34]. Hemicyanine dye (**8**) (140 mg, 0.25 mmol) was then dissolved in dry dichloromethane (7 mL) and stirred under N_2. Trimethylamine (0.5 mL) and Bop (110 mg, 0.5 mmol) were added to the mixture. After the reaction was stirred for 15 min, 2-aminophenylboronic acid pinacol ester (114 mg, 0.52 mmol) in 2 mL of dichloromethane was added. This reaction mixture was stirred at room temperature overnight under N_2. The solvent was removed and the crude product washed with water and brine solution, extracted with dichloromethane and dried over sodium sulfate. The solvent was evaporated and the crude product was purified by column chromatography with dichloromethane /methanol (v/v) 50:1 and then (v/v) 20:1 to produce the product as a green solid with 15% yield. ^{1}HNMR (400 MHz, Acetonitrile-d_3) δ: 8.13 (1H, d, J = 6 Hz), 8.04 (1H, m), 7.78 (2H, m), 7.45 (2H, m), 7.33 (3H, m), 7.11 (1H, m), 6.82 (1H, m), 6.71 (2H, m), 6.12 (2H, d, J = 12 Hz), 3.58 (3H, s), 3.53 (4H, m), 3.33 (1H, d, J = 6 Hz), 2.64 (2H, m), 2.37 (2H, t, J = 6 Hz), 1.76 (6H, s), 1.35 (8H,s), 1.29 (2H, d, J = 4.83), 1.23 (5H, m), 1.13 (2H, s); ^{13}CNMR (75 MHz, Acetonitrile-d_3) δ: 175.08, 168.32, 152.57, 136.63, 133.23, 132.25, 130.59, 130.18, 129.38, 128.90, 125.95, 124.30, 123.04, 119.70, 118.12, 116.58, 114.05, 112.68, 111.79, 96.90, 92.58, 85.49, 74.67, 50.26, 45.64, 32.20, 28.45, 27.53, 25.27, 21.33, 12.70.

2.2. Optical measurement

We investigated the effect of pH on the absorption spectra of the fluorescent probes. A citrate–phosphate buffer (0.1 M) was used for

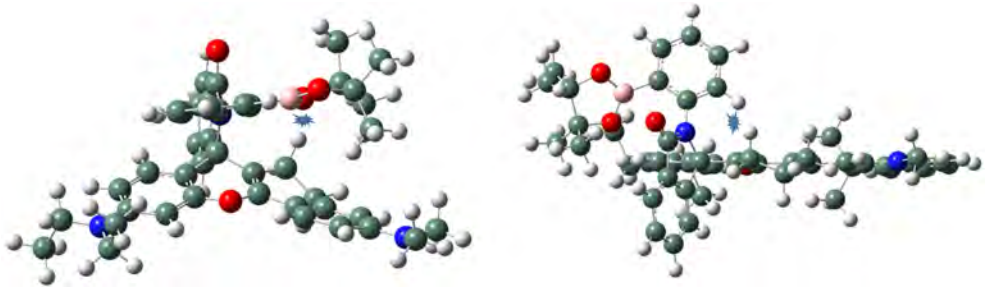

Fig. 3. GaussView [46] drawings of 5 μM probes **B** (left) and **C** (right) where the steric interactions are indicated with a .

acidic pH and a carbonate-bicarbonate buffer (0.2 M) was used for basic pH. Ethanol 1.0% was used as a co-solvent. The photostability and selectivity measurements of the fluorescent probes were conducted under similar conditions to those employed for the investigation of the pH dependency.

2.3. Live cell imaging

MDA-MB231 and HUVEC-C cells were obtained from ATCC and cultured according to published protocols [35]. For imaging experiments, cells were plated in 12 well plates at the seeding density of 1×10^5 cells/well and incubated overnight at 37° C in a 5% CO_2 incubator. The cells were then rinsed twice with 1 × PBS and subjected to serum starvation for two hours. Incubation with probe **A** (5 μM/10 μM), **B** (5 μM) and **C** (5 μM) were carried out for one hour in fresh serum free media containing 1 μM Lysosensor green DND-189 (Life Technologies) at 37 °C. Hoechst 33342, a nuclear stain (1 μg/mL) was added to the cells and allowed to incubate for 10 min. After incubation, cells were rinsed thrice with potassium rich PBS prepared at different pH values of 4.5, 5.5, 6.5, 7.5 or 8.5. The cells were further incubated with nigericin (1 μg/mL) for 5 min in potassium rich PBS buffers at different pHs [36,37]. Finally, the images were acquired using an inverted fluorescence microscope (AMF-4306, EVOSfl, AMG) at 60X magnification. Incubation of cells in serum free media can eliminate the known and unknown factors present in serum, minimize the analytical interference and offer more reproducible conditions [38].

2.4. Computational details

Models suitable for calculations for probes A-**C** and their protonated versions were obtained as described previously [39] using Chem3d with MM2 minimization of energies [40], followed by force field (UFF) calculations in Avogadro [41]. The molecular data were refined using density functional theory (DFT) employed with the APFD functional [42] and electron basis sets initially at the 6–31*g(d) level to convergence in Gaussian 16 [43]. The final model was conducted with 6–311 + g(2d,p) basis sets for all structures. Imaginary frequencies were not obtained in any of the frequency calculations. The excited states were assessed on the basis of TD-DFT optimizations [44] in a Polarizable Continuum Model (PCM) of water [45]. Results were

Table 1
Comparison of equivalent bond distances in the probe **A-C** and their protonated versions.

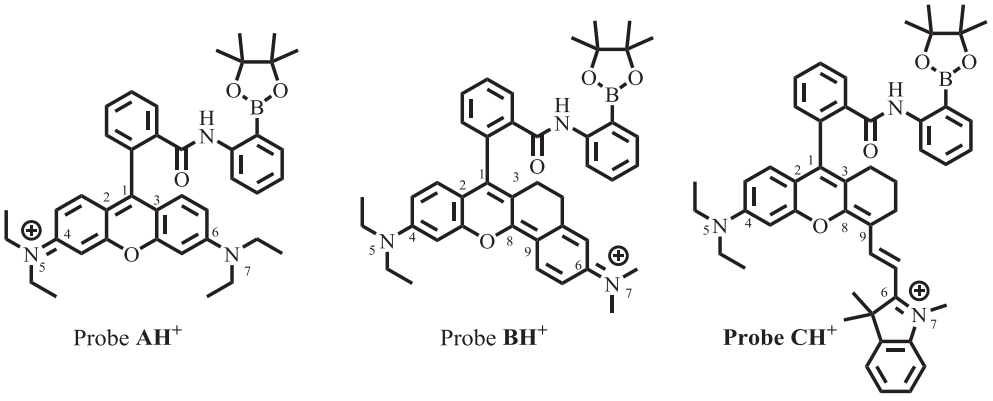

Bond distances	Probe A	Probe B	Probe C
1–2	1.503	1.498	1.498
1–3	1.507	1.505	1.507
4–5	1.366	1.366	1.367
6–7	1.365	1.375	1.376
8–9		1.455	1.454
Bond distances	Probe AH^+	Probe BH^+	Probe CH^+
1–2	1.401	1.409	1.415
1–3	1.398	1.384	1.377
4–5	1.343	1.348	1.359
6–7	1.343	1.348	1.349
8–9		1.421	1.406

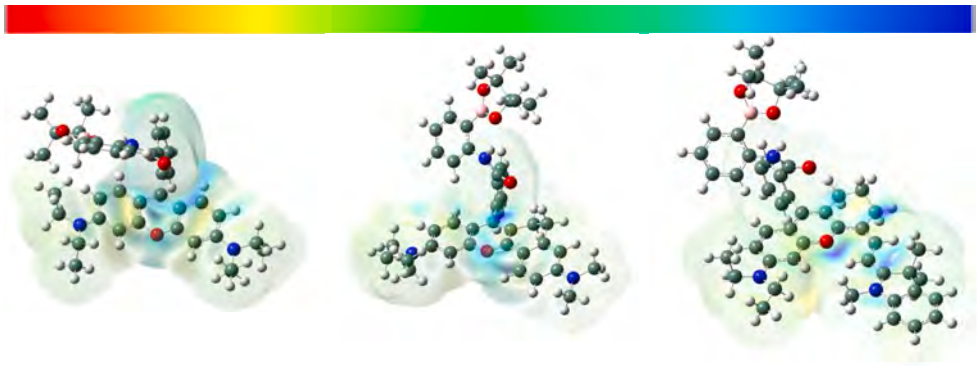

Fig. 4. Current density difference illustrations as *iso*-surfaces for probe $\mathbf{AH}^+$ (left), $\mathbf{BH}^+$ (middle) and $\mathbf{CH}^+$ (right) as indicated for the excited states (ES) and the calculated and (experimental) wavelength. The composition of that specific ES together with percentage contribution is also indicated. Drawings of the numbered linear combination of atomic orbitals (LCAOs) are available in Supporting Information. The different density color scale ranges are $\pm$ 7.562e^{-5} for $\mathbf{AH}^+$, $\pm$ 4.797e^{-5} for $\mathbf{BH}^+$ and $\pm$ 6.454e^{-5} for $\mathbf{CH}^+$, see scale at the top of the illustration with red negative and blue positive. (For interpretation of the references to color in this figure legend, the reader is referred to the web version of this article.)

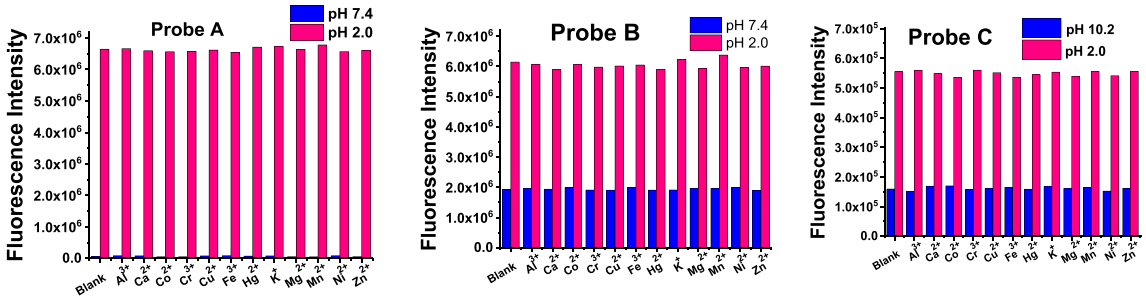

Fig. 5. Fluorescence responses of probes 5 μM **A**, **B** and **C** to pH in the absence and presence of cations and anions under excitation of 530 nm, 560 nm and 660 nm, respectively.

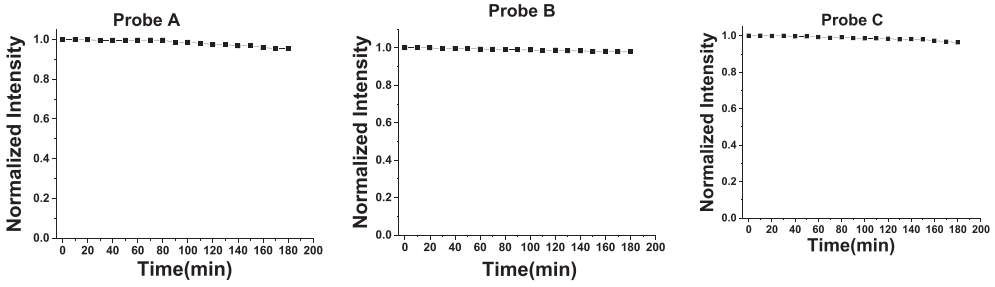

Fig. 6. Fluorescence intensities of 5 μM probes **A, B** and **C** in a pH 2.4 buffer under three-hour continual excitation of 530 nm, 560 nm, and 660 nm.

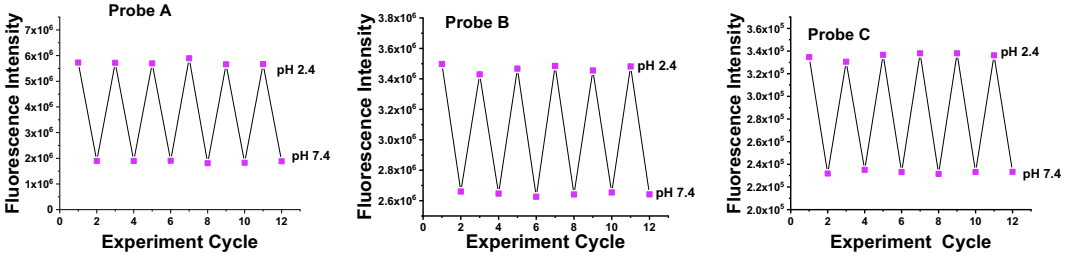

Fig. 7. The reversible responses of pH changes between pH 2.4 and 7.4 of 5 μM probes **A-C** under excitation of wavelength of 530 nm, 560 nm, and 660 nm respectively.

interpreted using GaussView 6 [46] for all data and figures. The results of the calculations (including drawings of LCAOs for all molecular orbitals discussed) are given in detail in the Supporting Information.

3. Results and discussion

3.1. Probe design and synthesis

We chose traditional rhodamine and its near-infrared derivative, and near-infrared hemicyanine dye as fluorophore probes not only because of their excellent photophysical properties including high extinction coefficient, high fluorescence quantum yields, and excellent photostability [9,30,47], but also their easy functionalization with amine derivatives to form different unique spirolactam molecular switches for different sensing and imaging applications. In order to increase pKa values of the fluorescent probes, we selected a considerably sterically bulky molecule, 2-aminophenylboronic acid pinacol ester, to modify these fluorophores. Traditional rhodamine B, Scheme

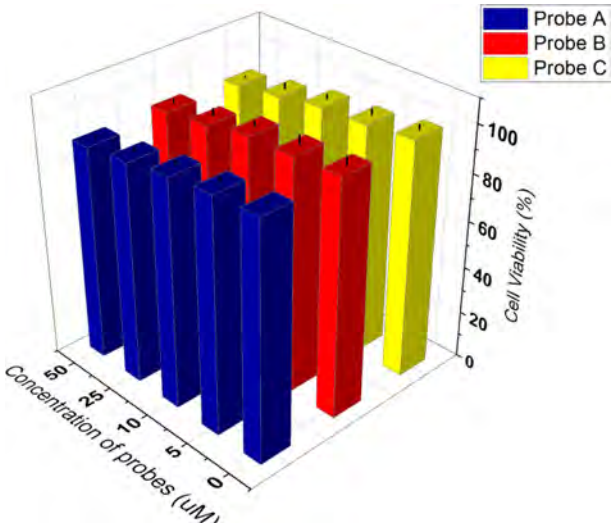

Fig. 8. Cytotoxicity of probes **A**, **B**, and **C** obtained by MTS assay. The HeLa cells were incubated with 0, 5, 10, 25, and 50 μM of probes **A**, **B**, and **C** for 48 h. The relative cell viability was normalized to untreated cells and the cell viability has a linear relationship with the absorbance at 490 nm. The error bars indicate ± SD.

2, is commercially available while a near-infrared rhodamine dye (**4**) was prepared by the condensation reaction of 6-(dimethylamino)-3,4-dihydronaphthalen-1(2H)-one (**3**) with 2-(4-(diethylamino)-2-hydroxybenzoyl) benzoic acid (**2**) in sulfuric acid at high temperature [26]. Near-infrared hemicyanine dye (**8**) was prepared by the condensation reaction of 2-(4-(diethylamino)-2-hydroxybenzoyl) benzoic acid (**2**) with cyclohexanone (**5**) in sulfuric acid at high temperature, affording 9-(2-carboxyphenyl)-6-(diethylamino)-1,2,3,4-tetrahydroxanthylium perchlorate (**6**) upon addition of perchloric acid, and followed by further condensation of intermediate (**6**) with Fisher's aldehyde (**7**). Fluorescent probes **A**, **B** and **C** were each prepared by coupling the carboxylic acid residues of rhodamine B, near-infrared rhodamine dye (**4**) and hemicyanine dye (**8**) respectively with 2-aminophenylboronic acid pinacol ester (**1**) in the presence of benzotriazol-1-yloxytris(dimethylamino)phosphonium hexafluorophosphate (BOP) reagent in methylene chloride containing triethylamine, see Scheme 2. The chemical structures of the probes were characterized by ^{1}H and ^{13}C NMR and electrospray ionization mass spectrometer (ESI-MS).

3.2. Absorption responses of the probes to pH changes

We obtained the absorption spectra of the probes in 0.1 M citrate–phosphate (pH 2.0 to 7.0) and phosphate-phosphate buffers (pH 7.0 to 10.8) containing 1% ethanol (Fig. 1). Probe **A** displays no absorption above 400 nm at neutral and basic pH environments as it retains a closed spirolactam configuration. Gradual pH decrease from 7.6 to 2.0 results in gradual absorbance increases of an absorption peak in now probe $\mathbf{AH}^{+}$ at 567 nm (Fig. 1). Probe **A** has a pKa value of 5.8 based on a plot obtained by titration of absorption and pH, Fig S19. Probe **B** has moderate absorption peak at 619 nm at basic pH 8.8, indicating that partial opening of the spirolactam ring configuration occurs under basic conditions due to the interactions between the sterically bulky 2-aminophenylboronic acid pinacol ester residue and the H atoms in the dihydronaphtyl moiety. Decreases of pH from 8.8 to 2.0 lead to substantial absorbance increases of the absorption peak at 619 nm. Probe **B** was assessed to have a similar pKa value at 5.5 compared to probe **A**, Fig S20. Probe **C** exhibits noticeable a near-infrared absorption peak at 724 nm and two short absorption peaks at 538 nm and 387 nm at a basic pH level of 10.8. Probe **C** responds to gradual pH decreases from 10.8 to 3.0 with significant absorbance increases of the near-infrared absorption peak, which is gradually blue shifted to a maximum of 10 nm upon attaining a pH of 3.0. Probe **C** has the highest pKa value of 6.31 among the three probes (Figs. S19–S21). The different pKa values of the probes can be ascribed to differences in the magnitude of steric hindrance between the closed spriolactam moiety, xanthene and its derivative cores and also the different nature of the conjugation obtained upon protonation.

We also evaluated fluorescence responses of the probes to pH changes in 0.1 M citrate–phosphate or phosphate buffer solutions containing 1% ethanol (Fig. 2). Via this method, probes **A-C** have pKa values of 5.81, 5.45 and 6.97, respectively as calculated using the Boltzmann equation, see Figs S16–S18. These pKa values obtained via fluorescence measurements are in good agreement with those obtained by absorption but these data had better R^2 values. Probe **A** based on traditional rhodamine B is non-fluorescent under neutral and basic pH conditions as it contains a closed spirolactam ring. Probe **A** reacts to pH decreases from 6.8 to 2.0 with significant fluorescence increases at 580 nm which is due to extended conjugation in the rhodamine moiety as a result of the opening of the spirolactam ring structure. In contrast, probes **B** and **C** show moderate fluorescence peaks at 650 nm and 740 nm at pH 8.8 and 10.8, respectively. Under basic pH conditions, a small percentage of probes **B** and **C** may exist in the protonated ring-opened spirolactam form and their moderate fluorescence may be due to their higher quantum yields compared to probe **A**. Probes **B** and **C** may possess larger steric hindrance between spirolactam rings and xanthene derivative moieties than probe **A**. Additionally our previously reported probe containing a xanthene derivative moiety and an adjacent ethylenediamine instead of the much larger aminophenylboronic acid pinacol ester group exhibited a pKa of 5.15 and was only fluorescent under acidic conditions [39]. Fluorescent probe based on near-infrared rhodamine dyes functionalized with o-phenylenediamine shows lower pKa values of 4.6 than probe **B** due to less steric hindrance between o-phenylenediamine residue from spirolactam ring and xanthene derivative moiety [23]. Fluorescent probe based on hemicyanine dye bearing o-phenylenediaimine residue in spirolactam ring also exhibits lower pKa value of 5.8 than probe **C** [8]. These comparative results convincingly indicate that use of 2-aminophenylboronic acid pinacol ester effectively increases pKa values of fluorescent probes based on spirolactam switches. Decreasing the pH from 8.8 to 2.0 (in probe **B**) and from 10.8 to 3.0 (in probe **C**) further activates ring opening of the spirolactam structures which significantly enhances fluorophore π-conjugation [23,25,48,49], and, consequently increases the fluorescence intensity of probe **B** and **C** at 650 nm and 740 nm, respectively.

3.3. Calculations

In order to understand the nature of any structural changes that the probes may experience upon protonation and to clarify the nature of the electronic transitions, theoretical calculations were conducted in Gaussian 16 [50] using the Austin-Frisch-Petersson functional with dispersion (APFD) [42]. TD-DFT optimizations [44] in a Polarizable Continuum Model (PCM) of water [45] were employed to calculate

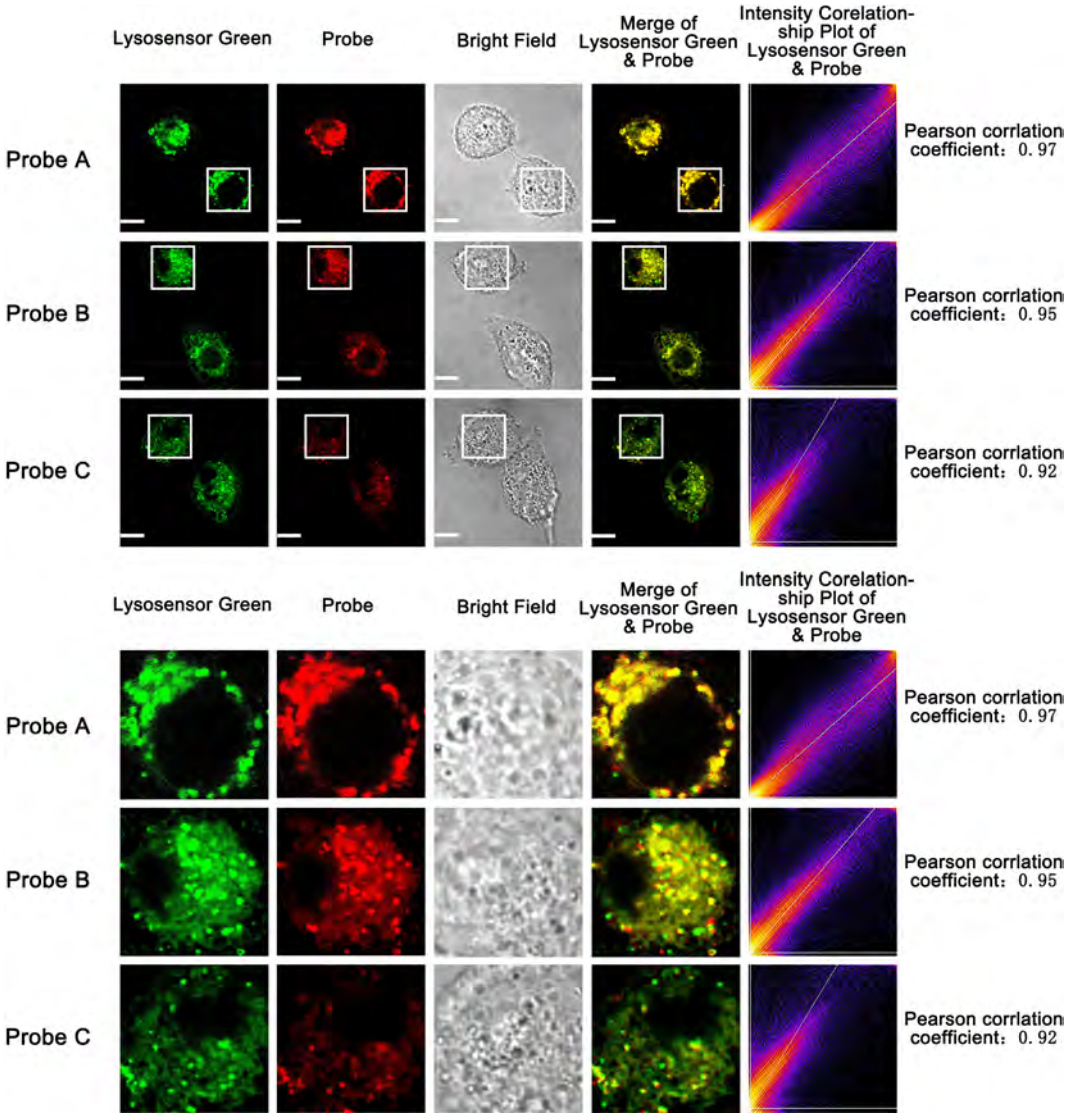

Fig. 9. Fluorescence images of probes **A, B** and **C** in HeLa cells were incubated with 5 μM probe **A, B** and **C** in pH 7.4 buffer. Lysosensor Green DND-189 (1 μM) were used for co-localization. The images were acquired using confocal fluorescence microscopy at 200X magnification and the scale bar is 20 μm. The excitation of Lysosensor Green was 488 nm and the images of Lysosensor Green were collected from 500 to 550 nm. For probe **A** and **B**, the excitation wavelength was 559 nm and the images were collected from 580 to 630 nm. For probe **C**, the excitation wavelength was 635 nm and the images were collected from 720 to 770 nm. Lower fluorescence images are enlarged images of the upper fluorescence images. (For interpretation of the references to color in this figure legend, the reader is referred to the web version of this article.)

excited states. Visible evidence of the hindrance between the 2-aminophenylboronic acid pinacol ester residue and an adjacent H atom in the xanthene derivative moieties in probes **B** and **C** is displayed in Fig. 3.

Comparing the optimized geometries of the probes **A-C** to the protonated versions $\mathbf{AH}^{+}$**–**$\mathbf{CH}^{+}$, as is presented in Figs. S25 to S31, Figs. S36 to S43 and Figs. S48 to S53, respectively, it is clear a more open structure was reached in the protonated probes as the N to C atom bond in the spirolactam ring breaks and the rhodamine part of the molecule become more conjugated. This can also be observed in the data listed in Table 1 which list a comparison of selected distances and reveals that shorter distances are obtained upon protonation. Specifically, there is a shortening of the bond distances in going from probe **A** to probe $\mathbf{AH}^{+}$ (Fig. 4).

There is also extended and equivalent resonance structures in the rhodamine moiety as the equal distances for 4–5 and 6–7 would indicate, see Table 1. However due to the insertion of the dihydronaphtyl moiety in probes **B** and **C**, evidence of the resonance structure depicted in Table 1 for these molecules is present in the different distances calculated for the equivalent bond lengths, in particular between 1 and 2 and 1–3. Interestingly there was no difference between 4–5 and 6–7 for probe **B** but in probe **C** a difference was obtained possible signifying a

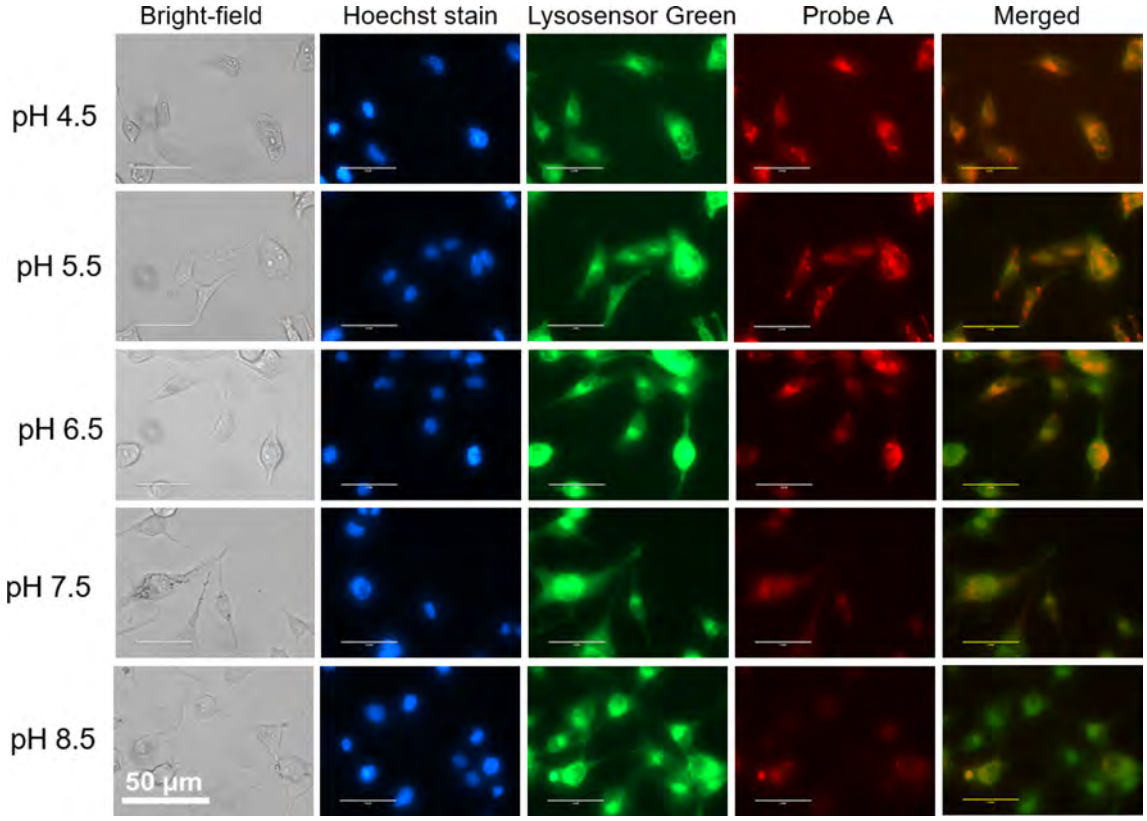

Fig. 10. Fluorescence images of 10 μM probe **A** in MDA-MB231 cells. MDA-MB231 cells were incubated with 10 μM probe **A** in buffers with different pH values ranging from pH 4.5 to 8.5 in presence of nigericin (1 μg/mL) for 1 h before imaging. Lysosensor Green DND-189 (1 μM) and Hoechst 33,342 (1 μg/mL) were used for co-localization. The images were acquired using an inverted fluorescence microscope (AMF-4306, EVOSfl, AMG) at 60X magnification. In the merged images, two channels of Lysosensor Green and the probe are merged together. (For interpretation of the references to color in this figure legend, the reader is referred to the web version of this article.)

more electron rich N atom at position 7.

We find transitions for probes **A** and **B** occur in the UV range as excited state 6 in Table S4 and excited state 4 in Table S8 occur at 300 and 327 nm, respectively. The addition of acid for these probes results in ring opening, a conjugated rhodamine moiety and a shift in the transition to the visible range calculated (expt) to be at 473 nm (567 nm) and 522 nm (619 nm) for probes $\mathbf{AH}^+$ and $\mathbf{BH}^+$ respectively. We find that the differences in thermal energies (with free energies in parenthesis) between the probes and their protonated versions are 8.88 (8.45), 8.14 (3.89) and 8.55 (6.61) kcals/mol for **A**, **B** and **C** respectively. These values suggest that it requires less energy to protonate probes **B** and **C** (note smaller ΔG values also) compared to probe **A**. For probe **C**, a transition at 388 nm as excited state 2 in Table S12 was calculated and involved π to π* orbitals on the hemicyanine moiety as the LCAOs in Figs. S51 and S52 indicates. The extended conjugation upon protonation to produce probe $\mathbf{CH}^+$ resulted in a transition at 591 nm (724 nm) listed as excited state 1 in Table S14. The nature of the conjugation is best summarized in an inspection of the current density diagrams which illustrates the direction of the electron flow from the HOMO to the LUMO. The illustration shows that electron density originates from the N atoms located at either end of the bottom section of the illustrations and moves towards the middle. The 2-aminophenylboronic acid pinacol ester residue is not involved with these transitions.

3.4. The selectivity of the probes

We investigated whether the probes react with 200 μM concentrations of various separate cations and anions in buffers at two different pH levels, namely, 2.0 and 7.4, see Fig. 5. There is no significant interference with probe responses to pH in the presence of cations such as Al^{3+}, Ca^{2+}, Co^{2+}, Cr^{3+}, Cu^{2+}, Fe^{3+}, Hg^{2+}, K^+, Mg^{2+}, Mn^{2+}, Ni^{2+} and Zn^{2+} ions, or anions such as Cl^-, Br^-, SO_3^{2-}, NO_2^-, NO_3^-, S^{2-}, CO_3^{2-} and HCO_3^-. These results indicate that the probes maintain high selective fluorescence responses to pH without interference from these cations and/or anions.

3.5. Probe photostability and their reversible responses to pH

We investigated the photostability of fluorescent probes **A**, **B** and **C** in a pH 2.4 buffer under three-hour continual excitation at 530 nm, 560 nm, and 660 nm, respectively. Fluorescent probes **A-C** showed excellent photostability with less than 4% decrease in fluorescence intensity during the three-hour excitation (Fig. 6). In addition, probes **A**, **B** and **C** show reversible response to pH change between 7.4 and 2.4 (Fig. 7).

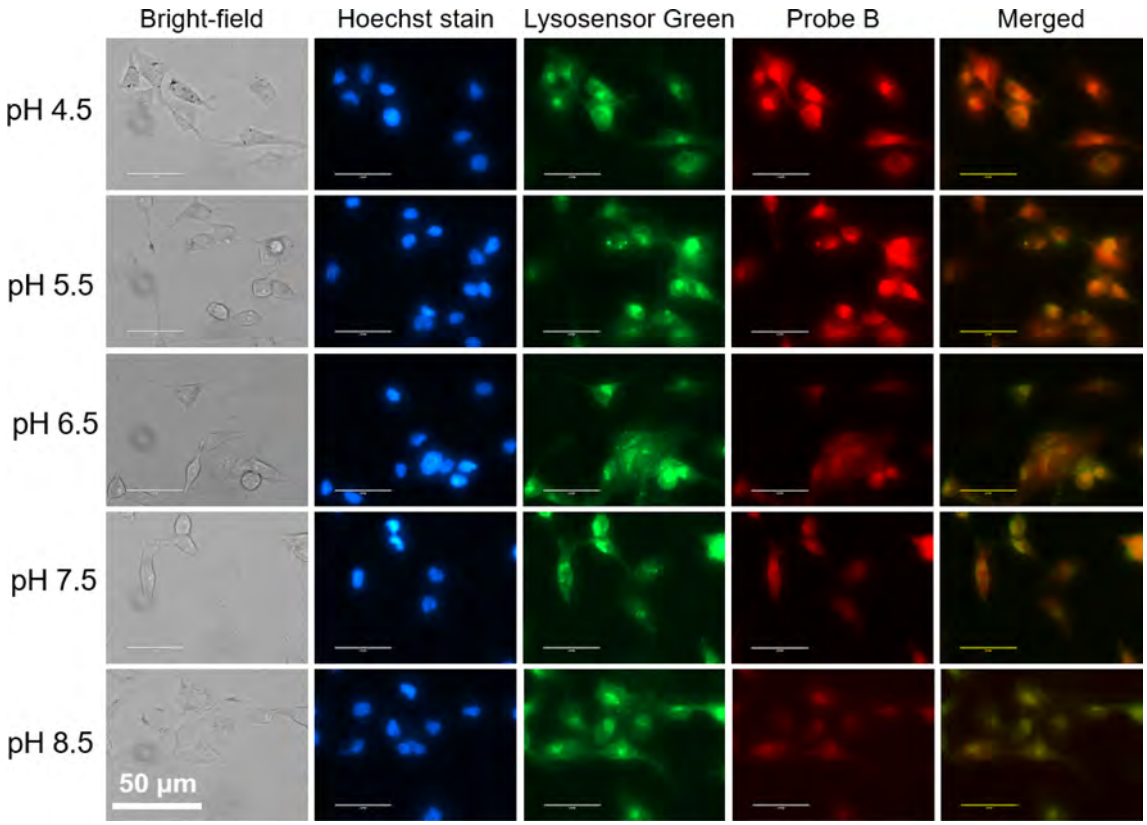

Fig. 11. Fluorescence images of 5 µM probe **B** in MDA-MB231 cells. MDA-MB231 cells were incubated with 5 µM probe **B** in buffers with different pH values ranging from pH 4.5 to 8.5 in presence of nigericin (1 µg/mL) for 1 h before imaging. Lysosensor Green DND-189 (1 µM) and Hoechst 33,342 (1 µg/mL) were used for co-localization. The images were acquired using an inverted fluorescence microscope (AMF-4306, EVOSfl, AMG) at 60X magnification. In the merged images, two channels of Lysosensor Green and the probe are merged together. (For interpretation of the references to color in this figure legend, the reader is referred to the web version of this article.)

3.6. Low cytotoxicity of the probes

An MTS assay was employed to evaluate the cytotoxicity of the probes with different concentrations from 5 µM to 50 µM for the viability of HeLa cells. We observed that cell viability values with 50 µM probes are higher than 82.3% suggesting no significant cytotoxicity occurs. Therefore, the low cytotoxicity and thus excellent biocompatibility allow for cellular imaging application (Fig. 8).

3.7. Live cell fluorescence imaging

We conducted cellular imaging of the probes by costaining breast cancer cell line (MDA-MB231) and human umbilical vein cells (HUVEC-C) with probes **A**, **B** and **C**, and a commercially available lysosome-targeting lysosensors Green DND-189 for co-localization analysis to determine whether the probes are located in the organelles of living cells (Fig. 9). The high Pearson's colocalization coefficients of more than 0.92 confirmed that the probes are localized in the lysosomes of living cells.

In order to quantitatively appraise fluorescence responses of the probes to intracellular pH changes, we incubated two different cell lines, breast cancer cell line (MDA-MB231) and HUVEC-C (see supplemental Figs. S58-S63) with the probes in different pH buffers from pH 4.5, 5.5, 6.5, 7.5, to 8.5 in the presence of 1 µg/mL nigericin ionophore, which is employed to exchange K^+ ions for H^+ ions across most cellular membranes, and equilibrate intracellular pH with extracellular pH in buffer solutions [8,21,23–25,27,37,51–53]. All cellular imaging for probe **A** were acquired by using an RFP light cube and for probes **B** and **C**, a CY5 light cube was used. The fluorescence intensity of probe **A** gradually becomes enhanced when the intracellular pH is lowered from 8.5 to 4.5 since pH decreases leads to opening of closed spirolactam ring of probe **A**, and enhance fluorescence of probe **A** with extended π-conjugation (Figures 10, S58, S61, S63, and S64). Probes **B** and **C** also respond to intracellular pH decreases from 8.5 to 4.5 with gradually fluorescence increases (Figures 11–12, S59-S63, S65, and S66). In contrast, Lysosensor Green is insensitive to intracellular pH changes (Figs. 10–12, S64–66). In all, zoomed in merged images (Figures S64-S66) show Hoechst 33342 stain marking the nuclear region and Lysosensor Green and Probe **A**/**B**/**C** co-localized (orange-yellow) in lysosomes and appear as punctate objects in the perinuclear region. This change in color (range is orange-yellow) is due to change in pH affecting fluorescence intensity of Probes **A**/**B**/**C** as pH changes, whereas intensity for Lysosensor Green does not change with change in pH (Figs. S64–S66). This co-localization of probes **A**/**B**/**C** with Lysosensor green and appearance of lysosomes as punctate objects is consistent with literature reports where in lysosomes are mostly found in the perinuclear region when serum-starved.

4. Conclusion

Three lysosome-targeting fluorescent probes (**A**, **B** and **C**) with high pK_a values of 5.81, 5.45 and 6.97 have been developed by coordination

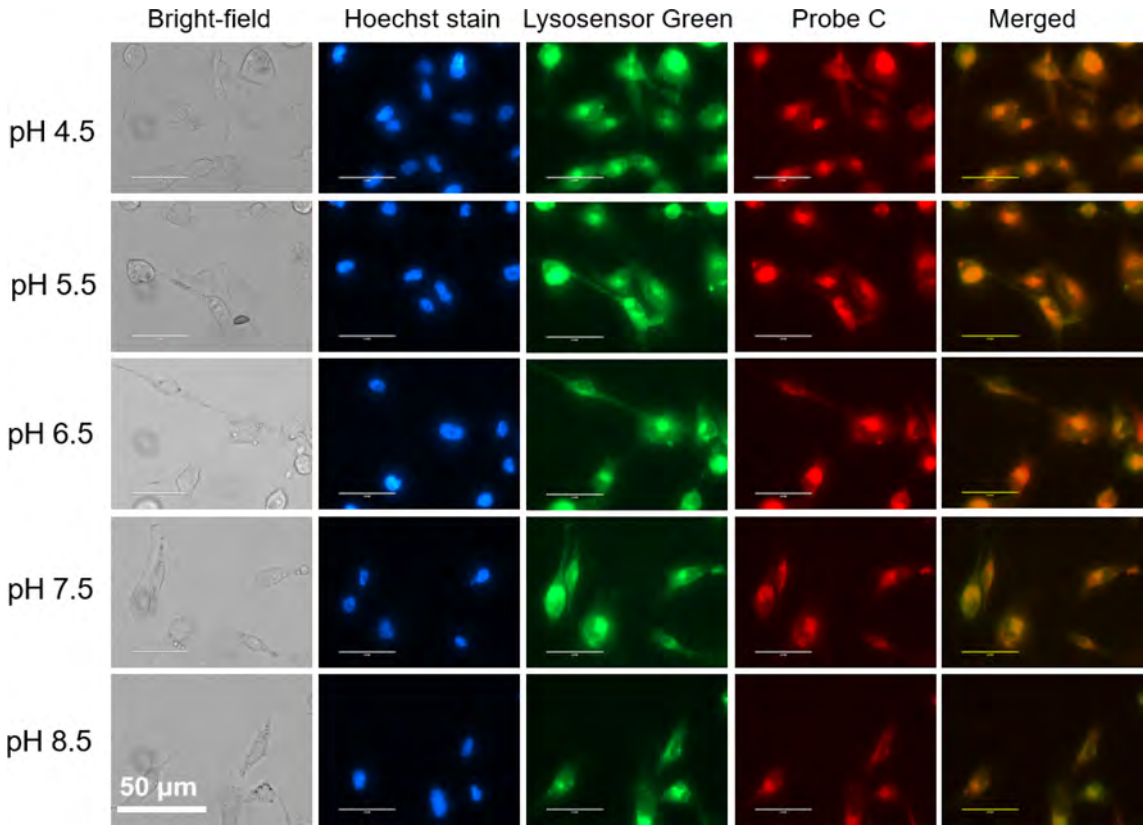

Fig. 12. Fluorescence images of 5 μM probe **C** in MDA-MB231 cells. MDA-MB231 cells were incubated with 5 μM probe **C** in buffers with different pH values ranging from pH 4.5 to 8.5 in presence of nigericin (1 μg/mL) for 1 h before imaging. Lysosensor Green DND-189 (1 μM) and Hoechst 33,342 (1 μg/mL) were used for co-localization. The images were acquired using an inverted fluorescence microscope (AMF-4306, EVOSfl, AMG) at 60X magnification. In the merged images, two channels of Lysosensor Green and the probe are merged together. (For interpretation of the references to color in this figure legend, the reader is referred to the web version of this article.)

of the sterically bulky 2-aminophenylboronic acid pinacol ester to traditional rhodamine, a near-infrared rhodamine dyes, and a near-infrared hemicyanine dye to form closed spirolactam ring structures. Probe **B** and **C** show moderate fluorescence with fluorescence quantum yields of 9% and 5% in neural pH 7.4 PBS buffer containing 1% ethanol. The probes have low cytotoxicity, excellent reversible pH responses, and high selectivity to pH over cations and anions. They have been applied to visualize intracellular pH changes in live cells.

Acknowledgements

This research was supported by the National Institute of General Medical Sciences of the National Institutes of Health under Award Number R15GM114751 and 2R15GM114751-02. Superior, a high-performance computing infrastructure at Michigan Technological University, was used in obtaining results presented in this publication.

Conflict of interest statement: None declared.

Appendix A. Supplementary data

Supplementary data to this article can be found online at https://doi.org/10.1016/j.ymeth.2019.07.012.

References

[1] H.-S. Lv, J. Liu, J. Zhao, B.-X. Zhao, J.-Y. Miao, Highly selective and sensitive pH-responsive fluorescent probe in living Hela and HUVEC cells, Sens. Actuators B Chem. 177 (2013) 956–963.
[2] J.R. Casey, S. Grinstein, J. Orlowski, Sensors and regulators of intracellular pH, Nat. rev. Mol. cell biol. 11 (1) (2010) 50.
[3] J. Han, K. Burgess, Fluorescent indicators for intracellular pH, Chem. Rev. 110 (5) (2009) 2709–2728.
[4] Y. Ge, D.F. O'Shea, Azadipyrromethenes: from traditional dye chemistry to leading edge applications, Chem. Soc. Rev. 45 (14) (2016) 3846–3864.
[5] S.C. Burleigh, T. van de Laar, C.J. Stroop, W.M. van Grunsven, N. O'Donoghue, P.M. Rudd, G.P. Davey, Synergizing metabolic flux analysis and nucleotide sugar metabolism to understand the control of glycosylation of recombinant protein in CHO cells, BMC Biotechnol. 11 (1) (2011) 95.
[6] V. Vingtdeux, M. Hamdane, S. Bégard, A. Loyens, A. Delacourte, J.-C. Beauvillain, L. Buée, P. Marambaud, N. Sergeant, Intracellular pH regulates amyloid precursor protein intracellular domain accumulation, Neurobiol. Dis. 25 (3) (2007) 686–696.
[7] S.-L. Shen, X.-P. Chen, X.-F. Zhang, J.-Y. Miao, B.-X. Zhao, A rhodamine B-based lysosomal pH probe, J. Mater. Chem. B 3 (5) (2015) 919–925.
[8] G.K. Vegesna, J. Janjanam, J. Bi, F.-T. Luo, J. Zhang, C. Olds, A. Tiwari, H. Liu, pH-activatable near-infrared fluorescent probes for detection of lysosomal pH inside living cells, J. Mater. Chem. B 2 (28) (2014) 4500–4508.
[9] S.G. Stratton, G.H. Taumoefolau, G.E. Purnell, M. Rasooly, W.L. Czaplyski, E.J. Harbron, Tuning the pKa of fluorescent rhodamine pH probes through substituent effects, Chem Eur. J. 23 (56) (2017) 14064–14072.
[10] L. Zhou, Y. Liu, S. Hu, H. Wang, H. Sun, X. Zhang, A new ratiometric two-photon fluorescent probe for imaging of lysosomes in living cells and tissues, Tetrahedron 72 (31) (2016) 4637–4642.
[11] L. Gerweck, K. Seetharaman, Cellular pH gradient in tumor versus normal tissue: potential exploitation for the treatment of cancer, Cancer Res. 56 (6) (1996) 1194–1198.
[12] B.L. Dong, X.Z. Song, X.Q. Kong, C. Wang, N. Zhang, W.Y. Lin, A tumor-targeting and lysosome-specific two-photon fluorescent probe for imaging pH changes in living cells, J. Mater. Chem. B 5 (5) (2017) 988–995.
[13] B.L. Dong, X.Z. Song, C. Wang, X.Q. Kong, Y.H. Tang, W.Y. Lin, Dual Site-controlled and lysosome-targeted intramolecular charge transfer-photoinduced electron transfer-fluorescence resonance energy transfer fluorescent probe for monitoring ph changes in living cells, Anal. Chem. 88 (7) (2016) 4085–4091.
[14] J.T. Hou, W.X. Ren, K. Li, J. Seo, A. Sharma, X.Q. Yu, J.S. Kim, Fluorescent bioimaging of pH: from design to applications, Chem. Soc. Rev. 46 (8) (2017) 2076–2090.
[15] Y.K. Yue, F.J. Huo, S. Lee, C.X. Yin, J. Yoon, A review: the trend of progress about pH probes in cell application in recent years, Analyst 142 (1) (2017) 30–41.
[16] R. Wang, C.W. Yu, F.B.A. Yu, L.X. Chen, Molecular fluorescent probes for monitoring pH changes in living cells, Trac-Trends Analy. Chem. 29 (9) (2010) 1004–1013.

[17] J. Yin, Y. Hu, J. Yoon, Fluorescent probes and bioimaging: alkali metals, alkaline earth metals and pH, Chem. Soc. Rev. 44 (14) (2015) 4619–4644.
[18] L. Yuan, W.Y. Lin, Z.M. Cao, J.L. Wang, B. Chen, Development of FRET-based dual-excitation ratiometric fluorescent ph probes and their photocaged derivatives, Chem. Eur. J. 18 (4) (2012) 1247–1255.
[19] H. Yu, G. Li, B. Zhang, X. Zhang, Y. Xiao, J. Wang, Y. Song, A neutral pH probe of rhodamine derivatives inspired by effect of hydrogen bond on pKa and its organelle-targetable fluorescent imaging, Dyes Pigm. 133 (2016) 93–99.
[20] R.Q. Zhang, F.Y. Yan, Y.C. Huang, D.P. Kong, Q.H. Ye, J.X. Xu, L. Chen, Rhodamine-based ratiometric fluorescent probes based on excitation energy transfer mechanisms: construction and applications in ratiometric sensing, RSC Adv. 6 (56) (2016) 50732–50760.
[21] D. Lee, K.M.K. Swamy, J. Hong, S. Lee, J. Yoon, A rhodamine-based fluorescent probe for the detection of lysosomal pH changes in living cells, Sens. Actuat. B-Chem. 266 (2018) 416–421.
[22] H.M. Li, C.L. Wang, M.Y. She, Y.L. Zhu, J.D. Zhang, Z. Yang, P. Liu, Y.Y. Wang, J.L. Li, Two rhodamine lactam modulated lysosome-targetable fluorescence probes for sensitively and selectively monitoring subcellular organelle pH change, Anal. Chim. Acta 900 (2015) 97–102.
[23] J.B. Wang, S. Xia, J.H. Bi, Y.B. Zhang, M.X. Fang, R.L. Luck, Y.B. Zeng, T.H. Chen, H.M. Lee, H.Y. Liu, Near-infrared fluorescent probes based on TBET and FRET rhodamine acceptors with different pK(a) values for sensitive ratiometric visualization of pH changes in live cells, J. Mater. Chem. B 7 (2) (2019) 198–209.
[24] Y.B. Zhang, J.H. Bi, S. Xia, W. Mazi, S.L. Wan, L. Mikesell, R.L. Luck, H.Y. Liu, A near-infrared fluorescent probe based on a FRET rhodamine donor linked to a cyanine acceptor for sensitive detection of intracellular pH alternations, Molecules 23 (10) (2018).
[25] Y.B. Zhang, S. Xia, M.X. Fang, W. Mazi, Y.B. Zeng, T. Johnston, A. Pap, R.L. Luck, H.Y. Liu, New near-infrared rhodamine dyes with large stokes shifts for sensitive sensing of intracellular pH changes and fluctuations, Chem. Commun. 54 (55) (2018) 7625–7628.
[26] G.L. Niu, P.P. Zhang, W.M. Liu, M.Q. Wang, H.Y. Zhang, J.S. Wu, L.P. Zhang, P.F. Wang, Near-infrared probe based on rhodamine derivative for highly sensitive and selective lysosomal pH tracking, Anal. Chem. 89 (3) (2017) 1922–1929.
[27] S.W. Zhang, T.H. Chen, H.M. Lee, J.H. Bi, A. Ghosh, M.X. Fang, Z.C. Qian, F. Xie, J. Ainsley, C. Christov, F.T. Luo, F. Zhao, H.Y. Liu, Luminescent probes for sensitive detection of pH changes in live cells through two near-infrared luminescence channels, ACS Sens. 2 (7) (2017) 924–931.
[28] S.G. Stratton, G.H. Taumoefolau, G.E. Purnell, M. Rasooly, W.L. Czaplyski, E.J. Harbron, Tuning the pK(a) of fluorescent rhodamine pH probes through substituent effects, Chem. Eur. J. 23 (56) (2017) 14064–14072.
[29] L. Yuan, W.Y. Lin, Y.M. Feng, A rational approach to tuning the pK(a) values of rhodamines for living cell fluorescence imaging, Organ. Biomol. Chem. 9 (6) (2011) 1723–1726.
[30] Y.-J. Gong, X.-B. Zhang, G.-J. Mao, L. Su, H.-M. Meng, W. Tan, S. Feng, G. Zhang, A unique approach toward near-infrared fluorescent probes for bioimaging with remarkably enhanced contrast, Chem. sci. 7 (3) (2016) 2275–2285.
[31] J.-Y. Xie, C.-Y. Li, Y.-F. Li, Y.-J. Fu, S.-X. Nie, H.-Y. Tan, A near-infrared chemosensor for determination of trivalent aluminum ions in living cells and tissues, Dyes Pigm. 136 (2017) 817–824.
[32] L. Yuan, W. Lin, Y. Yang, H. Chen, A unique class of near-infrared functional fluorescent dyes with carboxylic-acid-modulated fluorescence ON/OFF switching: rational design, synthesis, optical properties, theoretical calculations, and applications for fluorescence imaging in living animals, J. Am. Chem. Soc. 134 (2) (2012) 1200–1211.
[33] D.G. Churchill, Chemical structure and accidental explosion risk in the research laboratory, J. Chem. Educ. 83 (12) (2006) 1798–1803.
[34] L. Yuan, W.Y. Lin, S. Zhao, W.S. Gao, B. Chen, L.W. He, S.S. Zhu, A unique approach to development of near-infrared fluorescent sensors for in vivo imaging, J. Am. Chem. Soc. 134 (32) (2012) 13510–13523.
[35] S. Zhu, J. Zhang, J. Janjanam, J. Bi, G. Vegesna, A. Tiwari, F.-T. Luo, J. Wei, H. Liu, Highly water-soluble, near-infrared emissive BODIPY polymeric dye bearing RGD peptide residues for cancer imaging, Anal. Chim. Acta 758 (2013) 138–144.
[36] X.-X. Zhang, Z. Wang, X. Yue, Y. Ma, D.O. Kiesewetter, X. Chen, pH-sensitive fluorescent dyes: are they really pH-sensitive in cells? Mol. Pharm. 10 (5) (2013) 1910–1917.
[37] J.T. Zhang, M. Yang, W.F. Mazi, K. Adhikari, M.X. Fang, F. Xie, L. Valenzano, A. Tiwari, F.T. Luo, H.Y. Liu, Unusual fluorescent responses of morpholine-functionalized fluorescent probes to pH via manipulation of BODIPY's HOMO and LUMO energy orbitals for intracellular pH detection, ACS Sens. 1 (2) (2016) 158–165.
[38] K. Lambert, S.J. Pirt, Growth of human diploid cells (strain mrc-5) in defined medium – replacement of serum by a fraction of serum ultra-filtrate, J. Cell Sci. 35 (1979) 381–392.
[39] Y. Zhang, J. Bi, S. Xia, W. Mazi, S. Wan, L. Mikesell, R.L. Luck, H. Liu, A near-infrared fluorescent probe based on a FRET rhodamine donor linked to a cyanine acceptor for sensitive detection of intracellular pH alternations, Molecules 23 (10) (2018) 2679/1-2679/15.
[40] ChemBio3D, ChemBio3D http://www.cambridgesoft.com/software/chembio3d, 2012.
[41] M.D. Hanwell, D.E. Curtis, D.C. Lonie, T. Vandermeersch, E. Zurek, G.R. Hutchison, Avogadro: an advanced semantic chemical editor, visualization, and analysis platform, J. Cheminform. 4 (2012).
[42] A. Austin, G.A. Petersson, M.J. Frisch, F.J. Dobek, G. Scalmani, K. Throssell, A density functional with spherical atom dispersion terms, J. Chem. Theory Comput. 8 (12) (2012) 4989–5007.
[43] M.J. Frisch, G.W. Trucks, H.B. Schlegel, G.E. Scuseria, M.A. Robb, J.R. Cheeseman, J.V. Ortiz, J. Cioslowski, D.J. Fox, Gaussian 16, Gaussian, Inc., Wallingford CT, 2016.
[44] M.E. Casida, C. Jamorski, K.C. Casida, D.R. Salahub, Molecular excitation energies to high-lying bound states from time-dependent density-functional response theory: characterization and correction of the time-dependent local density approximation ionization threshold, J. Chem. Phys. 108 (11) (1998) 4439–4449.
[45] E. Cances, B. Mennucci, J. Tomasi, A new integral equation formalism for the polarizable continuum model: theoretical background and applications to isotropic and anisotropic dielectrics, J. Chem. Phys. 107 (8) (1997) 3032–3041.
[46] GaussView, V. 6, R. Dennington, T.A. Keith, J.M. Millam, Semichem Inc. Shawnee Mission, KS, 2016.
[47] Z.-Q. Hu, M. Li, M.-D. Liu, W.-M. Zhuang, G.-K. Li, A highly sensitive fluorescent acidic pH probe based on rhodamine B diethyl-2-aminobutenedioate conjugate and its application in living cells, Dyes Pigm. 96 (1) (2013) 71–75.
[48] S. Xia, J.B. Wang, J.H. Bi, X. Wang, M.X. Fang, T. Phillips, A. May, N. Conner, M. Tanasova, F.T. Luo, H.Y. Liu, Fluorescent probes based on pi-conjugation modulation between hemicyanine and coumarin moieties for ratiometric detection of pH changes in live cells with visible and near-infrared channels, Sens. Actuator B-Chem. 265 (2018) 699–708.
[49] S. Xia, M.X. Fang, J.B. Wang, J.H. Bi, W. Mazi, Y.B. Zhang, R.L. Luck, H.Y. Liu, Near-infrared fluorescent probes with BODIPY donors and rhodamine and merocyanine acceptors for ratiometric determination of lysosomal pH variance, Sens. Actuator B-Chem. 294 (2019) 1–13.
[50] M.J. Frisch, G.W. Trucks, H.B. Schlegel, G.E. Scuseria, M.A. Robb, J.R. Cheeseman, G. Scalmani, V. Barone, G.A. Petersson, H. Nakatsuji, R.L. Martin, K. Morokuma, O. Farkas, J.B. Foresman, D.J. Fox, Gaussian 16, Revision A.03, Gaussian Inc., Wallingford CT, 2016.
[51] M.X. Fang, R. Adhikari, J.H. Bi, W. Mazi, N. Dorh, J.B. Wang, N. Conner, J. Ainsley, T.G. Karabencheva-Christova, F.T. Luo, A. Tiwari, H.Y. Liu, Fluorescent probes for sensitive and selective detection of pH changes in live cells in visible and near-infrared channels, J. Mater. Chem. B 5 (48) (2017) 9579–9590.
[52] M.X. Fang, S. Xia, J.H. Bi, T.P. Wigstrom, L. Valenzano, J.B. Wang, W. Mazi, M. Tanasova, F.T. Luo, H.Y. Liu, A cyanine-based fluorescent cassette with aggregation-induced emission for sensitive detection of pH changes in live cells, Chem. Commun. 54 (9) (2018) 1133–1136.
[53] J.B. Wang, S. Xia, J.H. Bi, M.X. Fang, W.F. Mazi, Y.B. Zhang, N. Conner, F.T. Luo, H.P. Lu, H.Y. Liu, Ratiometric near-infrared fluorescent probes based on through bond energy transfer and pi-conjugation modulation between tetraphenylethene and hemicyanine moieties for sensitive detection of pH changes in live cells, Bioconjug. Chem. 29 (4) (2018) 1406–1418.